

# New Synchronous Orbits Using the Geomagnetic Lorentz Force

Brett Streetman\* and Mason A. Peck †

*Cornell University, Ithaca, New York 14853*

The Lorentz Augmented Orbits (LAO) concept provides propellantless electromagnetic propulsion without a tether, using the interaction between an electrostatically charged satellite and the Earth's magnetic field to provide a useful thrust. New types of Earth-synchronous orbits are found from equations governing the motion of satellites experiencing the Lorentz force in orbit. The equations of motion for such a spacecraft are derived based on a simplified magnetic field model, in which the dipole is aligned with true north. For a polar orbiting satellite, a constant electrical charge can create arbitrary changes in the right-ascension angle. This method allows for single-orbit repeat-groundtrack LEO satellites. Analytical expressions for changes in orbital elements due to Lorentz forces are verified by numerical simulation for the polar and equatorial cases. In the equatorial case, manipulation of the longitude of perigee by constant electrostatic charge is possible. Perigee movement also allows for the creation of an Earth-synchronous type of orbit.

## I. Introduction

A REPEAT groundtrack orbit is any orbit whose sub-satellite point traces out a recurring pattern in some integer numbers of orbits. Traditionally, these orbits are achieved by adjusting the period of a satellite such that it completes an integer number of orbits in exactly an integer number of sidereal Earth days. Geostationary and Geosynchronous orbits are perhaps the most familiar and useful examples. These orbits have a mean motion equal to the spin rate of the Earth. We shall refer to orbits that repeat their groundtrack every orbit as GT-1 orbits. Thus all GEO orbits are in the GT-1 class. We define a general notation of a GT- $x$  class orbit repeats its groundtrack every  $x$  orbits. For example, satellites in the GPS constellation are in 12 sidereal hour orbits, and can thus be considered GT-2 satellites. Many LEO imaging satellites designed for full-Earth coverage also use repeat track orbits. Landsat 7 covers the full Earth every 233 orbits making it a GT-233 satellite: every 16 days, the satellite completes exactly 233 orbits.<sup>1</sup>

Dedicated weather satellites and both government and commercial communications satellites are just a few of the numerous uses for GT-1 orbits. However GT-1 systems are currently limited to GEO orbits. The altitude of these satellites, roughly 36000km, requires high-power communications and impacts the aperture requirements for Earth-imaging satellites. An ideal arrangement would be a GT-1 orbit at a low Earth altitude. We propose a method of obtaining a low Earth, polar GT-1 orbit with the help of a new propellantless propulsion concept called Lorentz Augmented Orbits (LAO).

The Lorentz force experienced by a particle of charge  $q$  (Coulombs) moving through a magnetic field  $\vec{B}$  is given by

$$\vec{F}_L = q\vec{v}_r \times \vec{B} \quad (1)$$

where  $\vec{v}_r$  is the particle velocity with respect to the magnetic field. This force, named after Dutch physicist and Nobel Prize winner Hendrik Lorentz, is used to provided meaningful propulsive actuation in a Lorentz Augmented Orbit.<sup>2</sup> An LAO system makes use of the interaction between the Earth's geomagnetic field and an electrostatic charge built up on a satellite. Thus, LAO is a form of electromagnetic propulsion that does not require a tether. A tether system normally entails a long conductive wire, through which a current is forced. The drifting electrons in the tether provide the moving charged particles necessary for the Lorentz

\*Graduate Research Assistant, Department of Mechanical and Aerospace Engineering, 245 Upson Hall, AIAA Student Member.

†Assistant Professor, Department of Mechanical and Aerospace Engineering, 212 Upson Hall, AIAA Member.

force.<sup>3</sup> In LAO, the spacecraft itself becomes the moving charged particle, creating a current along its orbital path.

An LAO is achieved by a spacecraft that uses electrical power to build up a net electrostatic charge on its body, and this net charge causes an interaction between the geomagnetic field and the vehicle in the form of the Lorentz force. The magnitude and direction of the force are defined by the size and polarity of the charge on the satellite  $q$ , the velocity of the vehicle with respect to the magnetic field  $\vec{v}_r$ , and the strength and direction of the magnetic field  $\vec{B}$ :

$$\vec{F}_L = q(\vec{v} - \vec{\omega}_E \times \vec{r}) \times \vec{B} \quad (2)$$

where the position of the satellite is given by  $\vec{r}$ , and  $\vec{\omega}_E$  represents the Earth's angular velocity. In an inertial frame the geomagnetic field rotates with the Earth and has a velocity of its own.<sup>4</sup> The relative velocity,  $\vec{v}_r$ , that defines the Lorentz force is given as the difference between the absolute spacecraft velocity,  $\vec{v}$ , and the velocity of the magnetic field,  $\vec{\omega}_E \times \vec{r}$ . The power system of the satellite can then modulate the net charge to control the propulsive force.

The LAO concept is propellant-free propulsion. The energy stored in Earth's rotation is used to do work on the vehicle. The size of the force is limited only by charge-holding capacity (i.e. its self-capacitance) and power constraints of the satellite. However, the direction of thrust is fixed with respect to the velocity direction of the spacecraft and the direction of the magnetic field. This direction limitation is not so restrictive as to render the system useless, though. With appropriate planning and orbit design, many extremely useful applications can be realized using an LAO system. Described below are methods for changing orbital energy, changing orbit angular momentum (both magnitude and direction), and arbitrary control of right ascension and argument of perigee for certain situations. This control allows for the creation of certain new Earth-synchronous orbits.

## II. Related Work and Concept Overview

The Lorentz Augmented Orbit system builds on previous research in many fields. Some of this work is presented here, along with some of the issues and complexities inherent in the system and a possible system architecture for implementation of an LAO.

### A. Related Work

The contribution of the Lorentz force to orbiting bodies has been observed in natural planetary systems.<sup>5,6</sup> Schaffer and Burns have analyzed the dynamics of dust particles charged by the plasma environment around Jupiter. They have shown that the motions of these small charged grains can be greatly affected by Lorentz mechanics. This mechanism can be used to explain sparse, latitudinally thick rings found around Jupiter's main rings. While the fundamental dynamics of these particles is well understood, we seek applications for controlled-charge spacecraft in a variety of orbits.

Just as dust grains naturally achieve some nonzero charge around Jupiter, a satellite orbiting in a plasma environment will attain a static charge. Many Earth orbiting spacecraft, such as the SCATHA mission, have measured this effect.<sup>7</sup> Garrett and Whittelsey<sup>8</sup> present an overview of the natural charging that occurs in the Earth environment. Spacecraft in Earth orbit tend to naturally hold a negative charge, and this charging occurs with a small time constant (on the order of milliseconds).<sup>9</sup>

If we wish to control the charge on the spacecraft, it must exchange charge with the plasma environment in some way. One possible solution involves the uses of ion or electron beams. The use of these beams has been extensively studied in conjunction with research in both missile defense and ionospheric physics. An overview of beam effects on satellites can be found in Lai.<sup>10</sup> In fact, Hough<sup>11</sup> describes the trajectory perturbations on a ballistic missile due to Lorentz force. However, this work is the only study of the effect of the Lorentz force on a spacecraft's orbit that has been found by the authors. The LAO system for orbital control was first proposed by Peck.<sup>2</sup>

Other studies have proposed various ways to use charged spacecraft and magnetic field interactions for many applications. Schaub et al.<sup>9</sup> and Schaub<sup>12</sup> present the idea of Coulomb spacecraft formations (CSF). Satellites in a CSF formation are electrostatically charged, and some measure of formation control is provided by the Coulomb forces between the various satellites. The CSF system faces many of the same system architecture challenges as the LAO system. However, due to plasma interactions, a CSF is impractical in LEO, while an LAO is more effective in LEO where the magnetic field strength is greater.

Another electromagnetic formation system is proposed by Kong et al.<sup>13</sup> Their Electromagnetic Formation Flight system uses superconducting dipole electromagnets on individual satellites in a formation to actuate formation keeping. Interaction between these magnets and the geomagnetic field was not expressly considered in their study.

One further application of charged satellites in a magnetic field is given by Tikhonov.<sup>14</sup> He proposes the use of nonuniform charging on a satellite to control attitude via the Lorentz force. This idea faces many of the same challenges and dynamics as the LAO systems but will not be considered further here.

## B. Issues and Complexities in the LAO System

A convenient and highly simplified model of an LAO consists of the geomagnetic field as a simple dipole, the magnetic north pole and the true north pole perfectly aligned, and the space environment as a true vacuum. Of course, these simplifications neglect certain subtleties. The Earth's magnetic field is nonuniform and varies in time, and it is frequently described by a number of terms from a spherical-harmonic expansion. The solar wind causes large spatial and temporal deformations of the field. In addition, magnetic north does not align with true north; magnetic north is about  $10^\circ$  south of the true pole. Furthermore, because the field rotates with the Earth, the relationship between the two poles is not constant in an inertial frame. Using the simpler non-tilted dipole model allows for clean, simple analytical results to be obtained. These simple results provide both insight into the problem and a starting point for a more in-depth analysis.

The Earth's plasma environment is also difficult to model. Plasma composition, temperature, and density vary both spatially and temporally over a large range of values in ways that are currently unpredictable. The interactions between a charged satellite and the plasma are also difficult to model and are affected by these subtleties. So, predictions of the charge decay of a satellite are uncertain at best.

The scope of this introductory LAO study does not include most of the complexities listed above. Most cases here assume a non-tilted dipole geomagnetic field. The implementation of an LAO system is only briefly discussed, and most of the paper assumes that a required charge on the satellite can be delivered, regardless of plasma environment or power constraints. This paper focuses on the basic orbital dynamics of an LAO and presents dynamically interesting cases with applications inspired by these results. We focus on these applications in the hope that they may motivate further work in the practical aspects of building an LAO-capable spacecraft.

## C. Possible System Architecture

There appear to be many ways to achieve some level of charge on a spacecraft. The present study considers only the amount of charge, not how it is achieved. Any method that achieves a certain electrostatic charge on the satellite will bring about the same orbital dynamics. The design considerations then involve power consumption, environmental interaction, and impacts on mission operations. These impacts include the effects of having a highly charged bodies present on the other subsystems of the spacecraft. Such effects include communications interference, influences on power generation, and electrostatic discharge between components. We present one simple method of addressing these issues.

A possible system architecture is shown in Fig. 1. This system is somewhat reminiscent of a Van de Graaff generator.<sup>15</sup> A boom out one side of the satellite contains an electron gun. This electron gun interacts with the ambient plasma and expels a beam of electrons. The loss of electrons through the beam causes a net positive charge to build up on the satellite. A conductive sphere is placed around the main spacecraft bus to hold this charge. By Gauss's Theorem, no electrical field can exist inside this conductive shell, allowing the spacecraft's subsystems to operate without risk of arcing and other charge-related phenomena. The spherical shell is envisioned as a lightweight, inflatable structure. If the shell's material is transparent, a solar power system may be able to operate normally inside. Also, the communications subsystem of the spacecraft is placed out on the boom to avoid interference due to the large potential of the satellite.

How much charge can be maintained on such a system is a matter of considerable debate. More charge can be obtained both by a larger sphere and a higher potential. However a larger sphere translates to more mass. The mass of spherical shell increases with its radius squared, while its capacitance only increases linearly with radius. There exists an optimal sphere radius depending on the properties of the shell material. Increasing the potential on the sphere creates problems as well. As the voltage increases, the number of ambient plasma particles impacting the spacecraft increases, causing a larger power need to maintain a particular charge. A more efficient means of storing charge may be on a long, thin wire. A wire is nearly

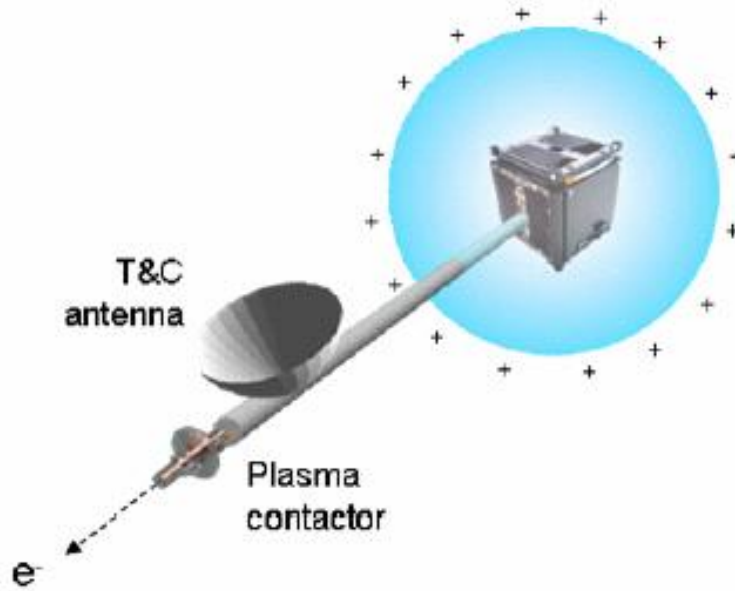


Figure 1. Possible LAO System Architecture

as effective at holding charge as a sphere, but can be made much less massive. The self-capacitance of a wire is generally given as  $4\pi\epsilon_0 L$ , where  $L$  is the length of the wire, while a sphere has a self-capacitance of  $4\pi\epsilon_0 R$ , where  $R$  is the sphere's radius. Effectively, the best way to store charge on an LAO spacecraft is a system that maximizes the average distance between charged particles, and thus the potential associated with them, while minimizing the mass of the storage apparatus. Since the mass of a wire increases with its length, adding wire increases charge to mass until the wire's mass begins to dominate the spacecraft system mass. At that point, the charge-to-mass asymptotes to the value for a wire alone. By contrast, the sphere's charge-to-mass cannot be increased arbitrarily. A reasonable estimate of maximum charge to mass ratio for the spherical construction and a 1 kg spacecraft bus is about  $4.4 \times 10^{-4}$  C/kg. A 10 km long, 1 mm radius wire on a 1 kg bus could possibly achieve a charge to mass ratio of about 0.1 C/kg. Allowing for thinner wires can greatly increase this value. The power required to combat incident plasma currents is not yet well understood, although estimates suggest that power, rather than capacitance, will ultimately limit the achievable charge-to-mass ratio.

### III. Equations of Motion

We derive equations of motion for the LAO system. These equations can include far more detailed models of magnetic field orientations and representations, but doing so obscures the fundamental behaviors for a minimal improvement in precision. We deal first with the simplified case of a single charged satellite in a dipole field that is not tilted with respect to the axis of rotation of the planet. This result is followed by a more general treatment of energy and angular momentum changes due to the Lorentz force.

#### A. Equations of Motion in a Non-tilted Dipole Field

The relevant vectors are represented in an Earth-centered, inertial spherical coordinate system. The spherical coordinates consist of radius  $r$ , colatitude angle  $\phi$ , and azimuth from the  $x$ -direction  $\theta$ , as shown in Fig. 2. The magnetic field is expressed as

$$\vec{B} = \frac{B_0}{r^3} [2 \cos \phi \hat{r} + \sin \phi \hat{\phi} + 0 \hat{\theta}] \quad (3)$$

The field rotates with the Earth. In the non-tilted field case,  $r$  and  $\phi$  are equivalent in both the rotating field frame and the inertial frame. As the dipole is axisymmetric, the magnetic azimuth does not directly

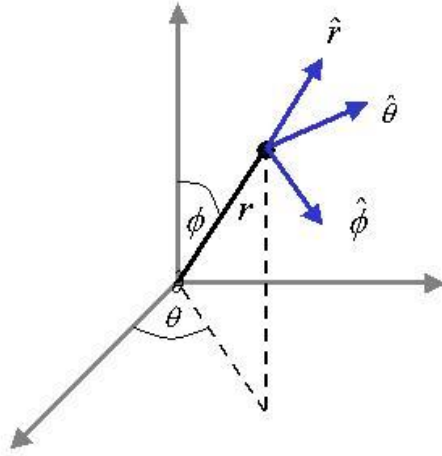


Figure 2. Spherical coordinates used in the derivation of the equations of motion.

contribute to the Lorentz force. For the Earth, the geographic North Pole is in fact the magnetic South Pole, hence the north side of a compass needle is attracted to the geomagnetic south pole. As we desire a coordinate system that has geographic north in the  $z$ -direction, we will be working with a dipole field that is essentially flipped upside down. We will correct for this fact by using a  $B_0$  term that is negative.

The acceleration in inertial coordinates is given by

$$\vec{a} = \vec{F}/m = -\frac{\mu}{r^3}\vec{r} + \frac{q}{m}(\vec{v} - \omega_E \hat{n}) \times \vec{r} \times \vec{B} \quad (4)$$

where  $\frac{q}{m}$  is the charge-to-mass ratio of the satellite in C/kg, and  $\hat{n}$  is a unit vector in the direction of the true north pole.

Expressing the Lorentz force (per unit mass) in the spherical, inertial frame yields

$$\vec{F}_L = \frac{q}{m}(\dot{\vec{r}} - \vec{\omega}_E \times \vec{r}) \times \vec{B} = q \left( \begin{bmatrix} \dot{r} \\ r\dot{\phi} \\ r\dot{\theta} \sin \phi \end{bmatrix} - \omega_E \begin{bmatrix} \cos \phi \\ -\sin \phi \\ 0 \end{bmatrix} \times \begin{bmatrix} r \\ 0 \\ 0 \end{bmatrix} \right) \times \frac{B_0}{r^3} \begin{bmatrix} 2 \cos \phi \\ \sin \phi \\ 0 \end{bmatrix} \quad (5)$$

which reduces to

$$\vec{F}_L = \frac{q}{m} \frac{B_0}{r^3} \begin{bmatrix} -r\dot{\theta} \sin^2 \phi + \omega_E r \sin^2 \phi \\ 2r\dot{\theta} \sin \phi \cos \phi - 2\omega_E r \cos \phi \sin \phi \\ \dot{r} \sin \phi - 2r\dot{\phi} \cos \phi \end{bmatrix} \quad (6)$$

Combining the Lorentz term with gravity and the standard accelerations in spherical coordinates gives the following three equations of motion:

$$\ddot{r} = r\dot{\theta}^2 \sin^2 \phi + r\dot{\phi}^2 - \frac{\mu}{r^2} - \frac{q}{m} \frac{B_0}{r^3} [r\dot{\theta} \sin^2 \phi - \omega_E r \sin^2 \phi] \quad (7)$$

$$r\ddot{\phi} = -2\dot{r}\dot{\phi} + r\dot{\theta}^2 \sin \phi \cos \phi + \frac{q}{m} \frac{B_0}{r^3} 2[r\dot{\theta} \sin \phi \cos \phi - \omega_E r \cos \phi \sin \phi] \quad (8)$$

$$r\ddot{\theta} \sin \phi = -2\dot{r}\dot{\theta} \sin \phi - 2r\dot{\phi}\dot{\theta} \cos \phi + \frac{q}{m} \frac{B_0}{r^3} [\dot{r} \sin \phi - 2r\dot{\phi} \cos \phi] \quad (9)$$

These three equations represent a sixth-order system that describes the motion of any orbit of a charged satellite in a non-tilted, dipole magnetic field.

## B. General Energy and Angular Momentum Change

The work-energy principle states

$$\dot{E} = \vec{v} \cdot \vec{F} \quad (10)$$

where  $E$  is the total energy of the system per unit mass,  $F$  is the applied force per unit mass, and  $v$  is the body's velocity. Including the Lorentz force gives

$$\dot{E} = \vec{v} \cdot \left( \frac{q}{m} \vec{v}_r \times \vec{B} \right) \quad (11)$$

Substituting for  $\vec{v}_r$  gives

$$\dot{E} = \vec{v} \cdot \left( \frac{q}{m} \vec{v} \times \vec{B} \right) - \vec{v} \cdot \left[ \frac{q}{m} (\omega_E \hat{n} \times \vec{r}) \times \vec{B} \right] \quad (12)$$

The  $\vec{v} \cdot (\vec{v} \times \vec{B})$  term is zero, yielding

$$\dot{E} = \frac{q}{m} \vec{v} \cdot \left[ \vec{B} \times (\omega_E \hat{n} \times \vec{r}) \right] \quad (13)$$

This result shows that only the rotation of the magnetic field allows the Lorentz force to do work on the satellite. A general magnetic force is conservative; thus the change in energy comes not from the magnetic field, but indirectly from the rotation of the Earth. Equivalently, a moving magnetic field is associated with an electric field, and this induced electric field can do work on a satellite.

Applying the triple cross product identity to Eq. 13 yields

$$\dot{E} = \frac{q}{m} \omega_E \left[ (\vec{v} \cdot \hat{n})(\vec{B} \cdot \vec{r}) - (\vec{v} \cdot \vec{r})(\hat{n} \cdot \vec{B}) \right] \quad (14)$$

This result is general. It describes any orbit or magnetic field configuration.

We can look at changes in the angular momentum in a similar way by examining the torques applied to the system by the Lorentz force, or

$$\dot{\vec{h}} = \vec{r} \times \vec{F} = \vec{r} \times \left( \frac{q}{m} \vec{v}_r \times \vec{B} \right) \quad (15)$$

where  $h$  is the angular momentum per unit mass of the system. Substituting for  $v_r$  and simplifying gives

$$\dot{\vec{h}} = \vec{r} \times \left( \frac{q}{m} \vec{v} \times \vec{B} \right) + \vec{r} \times \left( \vec{B} \times \left[ \frac{q}{m} \omega_E \hat{n} \times \vec{r} \right] \right) \quad (16)$$

Applying the triple cross product formula to both terms and simplifying further yields the following general expression:

$$\dot{\vec{h}} = \frac{q}{m} (\vec{B} \cdot \vec{r}) \vec{v} - \frac{q}{m} (\vec{r} \cdot \vec{v}) \vec{B} - \frac{q}{m} \omega_E (\vec{B} \cdot \vec{r}) (\hat{n} \times \vec{r}) \quad (17)$$

Depending on the orbital and magnetic configurations, we may change both the magnitude and direction of the angular momentum vector. Changing the direction of this vector will allow some measure of control over both the inclination and right ascension angle of the orbit. This control is examined in more detail for two cases below.

## IV. Applications

Using the Lorentz force in a beneficial way is sometimes not an intuitive exercise. The LAO system cannot control the the direction of the force, only magnitude and perhaps the sign, depending the implementation architecture. The force is also perpendicular to the field-fixed velocity of the spacecraft. Were the magnetic field not rotating, no energy could be added to an LAO. But with the rotating field, the energy and angular momentum of the orbit can be changed in most cases. And with appropriate control of the charge on the satellite, controlling energy and momentum allows for control over most of the orbital elements of the spacecraft. Two specific cases are developed below: the polar circular orbit and the general equatorial orbit, both in a non-tilted dipole field. Additionally, the relation between Lorentz and Earth oblateness effects will be examined and a comparison will be made between an electrodynamic tether system and an LAO.

## A. Polar Circular Orbit, Non-tilted Dipole Field

We apply the general energy and momentum relationships in Eqs. 14 and 17 to two specific cases to develop some simple and interesting results. First we examine a polar, circular orbit in a non-tilted dipole magnetic field. In this case the following expressions hold:

$$\vec{v} \cdot \vec{r} = 0; \quad \vec{B} \cdot \vec{r} = 2 \frac{B_0}{r^2} \sin u; \quad \vec{v} \cdot \hat{n} = v_c \cos u; \quad v_c = \sqrt{\frac{\mu}{r}} \quad (18)$$

where  $r$  is the radius of the orbit, and  $u$  is the argument of latitude of the satellite. The argument of latitude is the angular position of the satellite around the orbit measured from the right ascension of the vehicle in the equatorial plane. Using these results in Eq. 14 gives

$$\dot{E} = 2 \frac{q}{m} \omega_E B_0 \sqrt{\mu} r^{-5/2} \sin u \cos u \quad (19)$$

This expression is an odd, periodic function and, thus, contributes no secular change to the energy of the orbit. However, the radius of the orbit oscillates with a frequency of twice per orbit. For a general elliptical orbit, the total orbital energy can be expressed as a function of the semimajor axis:

$$E = -\frac{\mu}{2a} \quad (20)$$

where  $a$  is the semimajor axis, and in the circular case  $a = r$ . Differentiating this expression to find the change in radius with respect to energy gives

$$\dot{r} = 2 \frac{r^2}{\mu} \dot{E} \quad (21)$$

Using this equation and Eq. 19 gives a radius change throughout the orbit of

$$\dot{r} = 4 \frac{q}{m} \omega_E \frac{B_0}{\sqrt{\mu}} r^{-1/2} \sin u \cos u \quad (22)$$

For constant  $\frac{q}{m}$ , this expression is periodic over an orbit. The radial velocity (and thus eccentricity) remains small for a constant  $\frac{q}{m}$ , keeping the expressions in Eq. 18 valid. The simulation results below back up this assumption, showing that deviations in eccentricity and inclination remains small. However, if we choose control the charge as a function of the argument of latitude, a secular change in the radius (and eccentricity) of the orbit can be obtained.

Similarly, the angular momentum change of a circular polar LAO is examined using Eq. 17, with the following relationships

$$\vec{r} \cdot \vec{v} = 0; \quad \vec{B} \cdot \vec{r} = 2 \frac{B_0}{r^2} \sin u; \quad \vec{v} = \begin{bmatrix} -v_c \sin u \\ v_c \cos u \\ 0 \end{bmatrix} \quad (23)$$

where the circular speed of the orbit is given by  $v_c$ , and, in the last expression, an orthogonal coordinate system has been assumed with the  $x$ -direction along the line of nodes, the  $y$ -direction aligned with the north pole, and the  $z$ -direction necessarily along the orbit angular momentum vector. This coordinate system also leads to

$$\hat{n} = \begin{bmatrix} 0 \\ 1 \\ 0 \end{bmatrix}; \quad \vec{r} = r \begin{bmatrix} \cos u \\ \sin u \\ 0 \end{bmatrix}; \quad \hat{n} \times \vec{r} = r \begin{bmatrix} 0 \\ 0 \\ -\cos u \end{bmatrix} \quad (24)$$

Using all of these expressions in Eq. 17 and simplifying gives

$$\dot{\vec{h}} = 2 \frac{q}{m} \frac{B_0}{r^2} \begin{bmatrix} -v_0 \sin^2 u \\ v_0 \sin u \cos u \\ r \omega_E \sin u \cos u \end{bmatrix} \quad (25)$$

This expression represents the time rate of change of the angular momentum vector due to the Lorentz force, for a circular, polar LAO.

We use this vector derivative to define several scalar derivatives of interest, including the time rates of change of the inclination angle, the right ascension angle, and the magnitude of the angular momentum. First, the derivative of the scalar angular momentum magnitude is given by

$$\dot{h} = \dot{\vec{h}} \cdot \hat{h} = \dot{\vec{h}} \cdot \begin{bmatrix} 0 \\ 0 \\ 1 \end{bmatrix} \quad (26)$$

as our coordinate system has the initial angular momentum in the  $z$ -direction. This expression simplifies to

$$\dot{h} = 2 \frac{q}{m} \frac{B_0}{r} \omega_E \sin u \cos u \quad (27)$$

Thus, the magnitude of the angular momentum vector changes in a purely periodic manner under a constant charge.

The inclination angle  $i$  is defined in terms of the angular momentum vector  $\vec{h}$  by

$$\hat{n} \cdot \vec{h} = h \cos i \quad (28)$$

Differentiating this expression to find the time rate of change of  $i$  gives

$$\hat{n} \cdot \dot{\vec{h}} = \dot{h} \cos i - h \sin i \frac{di}{dt} \quad (29)$$

where the notation  $\frac{di}{dt}$  is used for clarity. Solving for  $\frac{di}{dt}$  and substituting in for the derivatives of angular momentum gives the following expression for time rate of change of inclination:

$$\frac{di}{dt} = \frac{-2 \frac{q}{m} \frac{B_0}{r^2} \sin u \cos u [v_0 - r \omega_E \cos i]}{rv_0 \sin i} \quad (30)$$

Again, for constant charge, this derivative is nonsecular, oscillating at a frequency of twice per orbit.

The line of nodes vector  $\vec{\Omega}$  is defined by

$$\vec{\Omega} = \hat{n} \times \vec{h} \quad (31)$$

and extends from the origin of the coordinate system through the point where the satellite ascends through the equatorial plane. Differentiating Eq. 31 gives

$$\dot{\vec{\Omega}} = \dot{\hat{n}} \times \vec{h} \quad (32)$$

which simplifies to

$$\dot{\vec{\Omega}} = -\frac{2qB_0}{mr^2} v_0 \sin^2 u \begin{bmatrix} 0 \\ 0 \\ 1 \end{bmatrix} + \frac{2q\omega_E B_0}{mr} \sin u \cos u \begin{bmatrix} 1 \\ 0 \\ 0 \end{bmatrix} \quad (33)$$

There are two terms in this derivative: one along the direction of the node vector, and one normal to it. The length of the node vector is irrelevant here. The term normal to the node vector is more interesting. It is in the equatorial plane, and thus represents a change in the right ascension angle  $\Omega$ . This term is an even function and produces a secular change. We can substitute into this expression the fact that the magnitude of the velocity in the circular orbit,  $v_c$ , is given by  $r\dot{u}$ . Thus the normal component of the vector right ascension change is

$$\dot{\vec{\Omega}}_n = -\frac{2qB_0}{mr} \sin^2 u \dot{u} \quad (34)$$

We can relate this to the actual angular right ascension change,  $\dot{\Omega}$ , by

$$\dot{\Omega} = \frac{\dot{\vec{\Omega}}_n}{\|\vec{\Omega}\|} \quad (35)$$

In this polar case, the magnitude of the node vector is simply the magnitude of the angular momentum vector, or

$$\|\vec{\Omega}\| = \|\vec{h}\| = r \sqrt{\frac{r}{\mu}} \quad (36)$$



because the angular momentum is perpendicular to the north direction. Equation 35 becomes

$$\dot{\Omega} = -2 \frac{q}{m} \frac{B_0}{r^2} \sqrt{\frac{r}{\mu}} \sin^2 u \dot{u} \quad (37)$$

This result represents the change in right ascension angle as a function of argument of latitude.

We can determine an average change in right ascension per orbit by integrating Eq. 37 around one complete orbit. The change in right ascension per orbit ( $\Delta\Omega$ ) is given by

$$\Delta\Omega = -2 \frac{q}{m} \frac{B_0}{r^2} \sqrt{\frac{r}{\mu}} \int_0^{2\pi} \sin^2 u \, du \quad (38)$$

which yields the following simple equation for change in right ascension per orbit:

$$\Delta\Omega = -2\pi \frac{q}{m} \frac{B_0}{r^2} \sqrt{\frac{r}{\mu}} \quad (39)$$

Thus, for the circular polar orbit, non-tilted dipole case, we can set an arbitrary change in right ascension per orbit. We can relate this to an average right ascension  $\Omega_{avg}$  change by multiplying by the period of the orbit:

$$\Delta\Omega = \Omega_{avg} \left( 2\pi \sqrt{\frac{r^3}{\mu}} \right) \quad (40)$$

Using this expression in Eq. 39 gives the following simple relationship between the charge to mass  $\frac{q}{m}$  and the average right ascension rate  $\Omega_{avg}$ , circular orbit radius  $r$ , and magnetic field strength  $B_0$ :

$$\frac{q}{m} = -\frac{\dot{\Omega}_{avg} r^3}{B_0} \quad (41)$$

We can now calculate the necessary charge-to-mass ratio for any desired right ascension rate.

Changing the right ascension of a polar orbit essentially amounts to changing longitude on the groundtrack of the satellite (see Fig. 3). Arbitrary right ascension control can greatly increase the efficiency of a polar

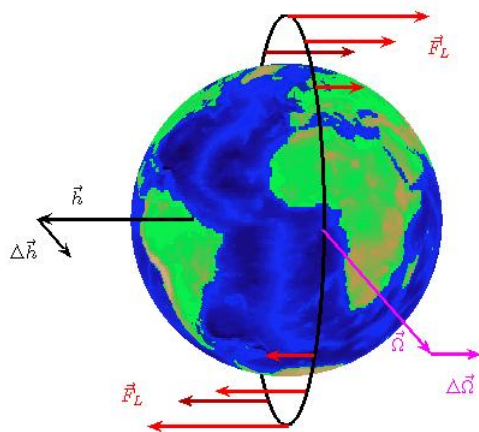


**Figure 3. Graphical representation of the vectors involved in an LAO GT-1 orbit.**

LEO imaging satellite. If full charge control is possible (both positive and negative charges) then the satellite can acquire a target faster, and then stay in the neighborhood of the target longer. In fact, if an average right ascension rate equal to the rate of Earth's rotation is acquired, then a satellite can have a single-orbit repeat-groundtrack. The satellite would pass over exactly the same points on the Earth every orbit. Thus, the orbit becomes a LEO GT-1 orbit. This groundtrack would allow a satellite to pass over an imaging target every 90 minutes rather than at most twice a day for an uncontrolled LEO polar satellite.

Solving for the required charge-to-mass ratio for an LAO GT-1 yields

$$\left(\frac{q}{m}\right)_{GT-1} = -\frac{\omega_E r^3}{B_0} \quad (42)$$

When evaluated for a circular orbit with 400km altitude, this expression reveals that a  $\frac{q}{m}$  of 2.831 C/kg is required for geosynchronous behavior. This  $\frac{q}{m}$  ratio is above the maximum limit for the simple architecture presented above, but it is not out of the realm of future possibilities.

Another possible application is a sun-synchronous LEO polar orbit at any altitude. The sun-synchronous condition is a right ascension rate of  $\dot{\Omega}_{ss} = 2\pi$  rad/year. As above, this yields a charge to mass for maintaining a sun-synchronous orbit of

$$\left(\frac{q}{m}\right)_{ss} = -\frac{\dot{\Omega}_{ss} r_0^3}{B_0} \quad (43)$$

For example, a 400km orbit requires a ratio 0.0078 C/kg for sun-synchronicity. This charge-to-mass ratio is well within the capabilities of near-term technologies.

The non-periodic change in right ascension persists for orbits that are not necessarily polar or circular. By extending the process outlined above to a general orbit (still assuming a non-tilted dipole field), an expression analogous to Eq. 41 is found for a general orbit:

$$\frac{q}{m} = \frac{\dot{\Omega}_{avg} a^3}{B_0} (1 - e^2)^{3/2} \frac{1}{\omega_E \sqrt{\frac{a^3}{\mu}} (1 - e^2)^2 \cos i \frac{e^2 - [(1 - e^2)^{1/2} - 1]^2 \cos 2\omega}{e^2} - 1} \quad (44)$$

This result is valid for any elliptical orbit under the influence of a non-tilted dipole.

## B. Equatorial Orbit, Non-tilted Dipole Field

A second simple case to consider is an equatorial orbit in a non-tilted dipole field. The true equator and the magnetic equator are aligned in this situation, and magnetic field is perpendicular to these planes. The eccentricity can be non-zero in this case.

The following relationships hold:

$$\vec{v} \cdot \vec{n} = 0; \vec{B} \cdot \hat{n} = -\frac{B_0}{r^3}; \vec{r} \cdot \vec{v} = \sqrt{\mu a(1 - e^2)} \frac{e \sin \nu}{1 + e \cos \nu} \quad (45)$$

where  $a$  is the orbit semimajor axis,  $e$  is the orbital eccentricity, and  $\nu$  is the true anomaly. Using these expressions, and the standard conic section equation for an elliptical orbit

$$r = \frac{a(1 - e^2)}{1 + e \cos \nu} \quad (46)$$

in Eq. 14 gives

$$\dot{E} = \frac{q}{m} \omega_E B_0 \sqrt{\mu} [a(1 - e^2)]^{-5/2} e \sin \nu (1 + e \cos \nu)^2 \quad (47)$$

Note the dependence on the eccentricity  $e$ . The lorentz force can add no energy to a circular equatorial orbit. Differentiating Eq. 20 gives a time rate of change of semimajor axis of

$$\dot{a} = 2 \frac{q}{m} e a^2 \omega_E \frac{B_0}{\sqrt{\mu}} [a(1 - e^2)]^{-5/2} \sin \nu (1 + e \cos \nu)^2 \quad (48)$$

Again, this change is nonsecular, but with proper modulation of  $\frac{q}{m}$ , the size of the equatorial orbit can be controlled using the Lorentz force.

Following the same procedure we can solve for the angular momentum change for the equatorial orbit. Using these relationships:

$$\vec{B} \cdot \vec{r} = 0; \vec{B} = \frac{B_0}{r^3} \begin{bmatrix} 0 \\ 0 \\ -1 \end{bmatrix} \quad (49)$$

with  $\vec{h}$  in the  $z$ -direction and Eq. 17 gives

$$\dot{\vec{h}} = -\frac{q}{m}(\vec{r} \cdot \vec{v})\frac{B_0}{r^3} \begin{bmatrix} 0 \\ 0 \\ -1 \end{bmatrix} \quad (50)$$

As this derivative only has a component in the  $z$ -direction, it represents only a change in the scalar magnitude of  $\vec{h}$ :

$$\dot{h} = \frac{q}{m}\frac{B_0}{r^3}(\vec{r} \cdot \vec{v}) \quad (51)$$

Substituting in Eqs. 46 and 45 gives

$$\dot{h} = \frac{q}{m}B_0\sqrt{\mu} [a(1 - e^2)]^{-5/2} e \sin \nu(1 + e \cos \nu)^2 \quad (52)$$

which is another periodic function with no secular terms. Here, the direction of  $h$  cannot be controlled, which means the inclination and right ascension angle cannot be changed.

We can derive the change in orbital eccentricity based on the following equation given by Burns:<sup>16</sup>

$$\dot{e} = \frac{1}{2e}(e^2 - 1) \left[ \frac{2\dot{h}}{h} + \frac{\dot{E}}{E} \right] \quad (53)$$

Applying our expressions for orbital energy and angular momentum change in Eqs. 47 and 52, respectively, gives

$$\dot{e} = -\frac{q}{m}B_0\frac{\sin \nu(1 + e \cos \nu)^2}{[a(1 - e^2)]^{3/2}} \left[ \frac{1}{a^{3/2}(1 - e^2)^{1/2}} - \frac{\omega_E}{\sqrt{\mu}} \right] \quad (54)$$

which is periodic in true anomaly. We can change the eccentricity of an initially circular orbit. So if we start with an initially circular orbit we first change the eccentricity and then can control the energy. Also from Burns,<sup>16</sup> we develop an expression for change in the argument of perigee,  $\omega$ , using the equation

$$\dot{\omega} = \dot{u} + \left( \frac{1}{r} - \frac{E}{e\mu} \cos \nu \right) \frac{2h\dot{h}}{e\mu \sin \nu} - \frac{h^2}{(e\mu)^2} \dot{E} \cot \nu \quad (55)$$

where  $\dot{u}$  represents an instantaneous change in the argument of latitude. For an equatorial orbit  $u$  is undefined but can be replaced by an equivalent angle measured from an inertial vector in the equatorial plane. As the satellite's position does not change in an instantaneous application of the Lorentz force, this inertial angle does not change either, leading to the  $\dot{u}$  term being zero. Again applying Eqs. 47 and 52 gives

$$\dot{\omega} = \frac{q}{m}B_0\frac{(1 + e \cos \nu)^2}{[a(1 - e^2)]^{3/2}} \left[ 2\frac{1 + e \cos \nu}{[a(1 - e^2)]^{3/2}} + \frac{\cos \nu}{a^{3/2}e(1 - e^2)^{1/2}} - \frac{\omega_E \cos \nu}{e\sqrt{\mu}} \right] \quad (56)$$

The first term in brackets of this equation gives rise to a secular change in the argument of perigee for a constant charge-to-mass ratio. This secular perigee change has many interesting, if somewhat esoteric, applications. Perigee control allows for the cancelation of various natural perturbation on the argument of perigee, such as J2 effects and lunar and solar tides. Another use may be to create a Molniya-type orbit at zero inclination (and most likely other inclinations). Building on the same ideas as the GT-1 LAO orbits discussed above, controlling perigee change not only can cancel out natural perturbations but also can match the earth's rotation. The line of apsides of such an orbit would remain at a constant longitude on Earth's surface. Thus, LAO creates possibilities for other kinds of synchronous orbits rather than just GT- $x$  orbits.

To evaluate this concept of precessing the line of apsides, we seek an expression for the  $\frac{q}{m}$  necessary to generate a certain average perigee change. First, we recognize that

$$\dot{\nu} = \frac{\sqrt{\mu}(1 + e \cos \nu)^2}{[a(1 - e^2)]^{3/2}} \quad (57)$$

by differentiating Eq. 46 and applying conservation of momentum. Substituting this expression into Eq. 56 gives

$$\frac{d\omega}{dt} = \frac{q}{m}\frac{B_0}{\sqrt{\mu}} \left[ \frac{2}{[a(1 - e^2)]^{3/2}} + \frac{2e \cos \nu}{[a(1 - e^2)]^{3/2}} + \frac{\cos \nu}{a^{3/2}e(1 - e^2)^{1/2}} - \frac{\omega_E \cos \nu}{e\sqrt{\mu}} \right] \frac{d\nu}{dt} \quad (58)$$

To find the change in perigee over one orbit, we recognize that this differential equation is separable and integrate both sides, varying  $\nu$  from 0 to  $2\pi$ . The integral over  $2\pi$  for all terms that depend solely on  $\cos \nu$  is zero leaving only

$$\Delta\omega = \frac{4\pi \frac{q}{m} B_0}{\sqrt{\mu} [a(1 - e^2)]^{3/2}} \quad (59)$$

For a certain desired rate of change in the argument of perigee  $\dot{\omega}_{des}$  we require that  $\Delta\omega/\Delta t = \dot{\omega}_{des}$ , where we set  $\Delta t$  to be one orbital period. Setting the resulting expression for  $\Delta\omega$  equal to Eq. 59 and solving for  $\frac{q}{m}$  gives a required charge to mass for some desired rate of perigee change:

$$\frac{q}{m} = \frac{\dot{\omega}_{des} a^3 (1 - e^2)^{3/2}}{2B_0} \quad (60)$$

This equation has similar dependencies as Eq. 41, the charge to mass required for a particular right ascension change for a polar circle. However, in the equatorial case, the eccentricity plays an important role in the magnitude of charge required. A higher eccentricity corresponds to a higher velocity at perigee for a given orbit size, which makes a more effective use of the Lorentz force, allowing for a smaller charge-to-mass ratio. Equation 60 applies for any desired rate of change for argument of perigee, including mitigating oblateness and third-body effects as well as introducing synchronous behavior. However, larger rates introduce inaccuracy in the  $\frac{q}{m}$  predicted by this osculating-elements approach. The derivation of this expression assumes that all the other orbital elements are changing slowly or are not explicit functions of  $\nu$ , and this may not be the case with a large charge-to-mass ratio.

The secular change in argument of perigee under a constant charge also arises in non-equatorial orbits. Following the same method as above, but generalized for any elliptical orbit, yields an expression for the charge to mass required for a desired perigee rate:

$$\frac{q}{m} = \frac{\dot{\omega}_{des} a^3 (1 - e^2)^{3/2}}{B_0 \cos i} \left[ 3 - \omega_E \sqrt{\frac{a^3}{\mu}} (1 - e^2)^2 \cos i \frac{e^2 - [(1 - e^2)^{1/2} - 1]^2 \cos 2\omega}{e^2} \right]^{-1} \quad (61)$$

A subtlety in the derivation of this expression arises from the  $\dot{u}$  term in Eq. 55. For an inclined orbit, this angle changes instantaneously only due to changes in the right ascension.<sup>16</sup> Thus the term  $\dot{u}$  becomes  $(-\cos i \dot{\Omega})$ , hence the similarities between Eq. 61 and Eq. 44.

Equation 61 gives the time rate of change of perigee relative to an inertial coordinate system. This change is the superposition of two different rates: the rate of change of argument of perigee within the orbit plane, and the change in perigee due to the fact that the right ascension, and thus orbital plane itself, is changing. In order to create the  $\omega$ -synchronous orbit described above, the rate of in-plane perigee change must be equal to the rotation rate of the Earth. Subtracting off the right ascension-caused rates gives

$$\frac{q}{m} = \frac{\omega_E a^3 (1 - e^2)^{3/2}}{2B_0 \cos i} \quad (62)$$

which differs only by a factor of  $\cos i$  from Eq. 60. Again, Eq. 62 is only valid for situations where desired rate of perigee change is based on a relationship with the rotating Earth, rather than some absolute inertial rate.

### C. Mitigation of Earth Oblateness Effects

The non-sphericity of the Earth causes secular changes in both the right ascension and argument of perigee of a spacecraft, herein referred to J2 effects.<sup>1</sup> The generally accepted secular time rates of change due to J2 are given as

$$\dot{\Omega}_{J2} = -3/2 \frac{J_2 R_E^2 \sqrt{\mu u}}{a^{7/2}} \frac{\cos i}{(1 - e^2)^2} \quad (63)$$

$$\dot{\omega}_{J2} = 3/4 \frac{J_2 R_E^2 \sqrt{\mu u}}{a^{7/2}} \frac{4 - 5 \sin^2 i}{(1 - e^2)^2} \quad (64)$$

It is trivial to use LAO to cancel the effect of J2 either the right ascension angle or the argument of perigee. The rate calculated with Eq. 63 or Eq. 64 can simply be substituted into Eq. 44 or Eq. 61, respectively. For

example, in an equatorial orbit with perigee at 400 km altitude and apogee at 1500 km, J2 will cause the argument of perigee to change by about 12.4°/day. The charge to mass required to overcome this change is about 0.042 C/kg, a reasonably small value.

There also exist orbits such that a constant charge LAO can cancel both the  $\Omega$  and  $\omega$ . These orbits can exist only below the J2 critical angle of  $i \approx 63.4^\circ$  or above the critical solution of  $i \approx 116.6^\circ$ . Additionally, the effect of the Lorentz force must be equivalent to the J2 effects in both the right ascension and the argument of perigee. This condition is true when the orbit in question satisfies the following expression:

$$\frac{3 - K}{1 - K} = \frac{4 - 5\sin^2 i}{2\cos^2 i} \quad (65)$$

where  $K$  is given by

$$K = \omega_E \sqrt{\frac{a^3}{\mu}} (1 - e^2)^2 \cos i \frac{e^2 - [(1 - e^2)^{1/2} - 1]^2 \cos 2\omega}{e^2} \quad (66)$$

While this equation does not easily yield simple relationships among the orbital elements, a minimum semimajor axis for this condition can be found. Under the most optimistic assumptions, namely  $e = 0$ , the expression in Eq. 65 can only be satisfied if the polynomial

$$3 \frac{w_E}{n} \cos^3 i + \cos^2 i - \frac{w_E}{n} \cos i + 1 = 0 \quad (67)$$

where  $n$  is the mean motion, has a valid solution. These solutions only exist when  $w_E/n > 1$ . Thus the orbit must have a semimajor axis outside of GEO in order to fully cancel J2 effects with a constant charge. At these altitudes, the J2 and LAO effects would generally not be the dominant perturbative forces on the satellite.

#### D. Tether/LAO Comparison for GT-1 Behavior

Electrodynamic tethers have long been examined as propellantless electromagnetic propulsion system. Under certain tether dynamics assumptions, a tether system can outperform an LAO system for some applications. However, for the LAO GT-1 synchronous orbits developed in Section A, we show a tether to be an infeasible method of propulsion.

In order for a tether to show polar GT-1 behavior, the tether current (and tether) must be in the along-track direction of the satellite. Although the flexible-body dynamics of a tether along the velocity direction of the spacecraft are non-trivial, here only the electrodynamic considerations will be addressed.

With an along-track electrodynamic tether, the Lorentz force experienced by the tether is equivalent to the Lorentz force on an LAO satellite. These two terms can be equated as

$$q\vec{v} \times \vec{B} = L\vec{J} \times \vec{B} \quad (68)$$

where the left side of the equation represents an LAO satellite, and the right a tether, with  $L$  being the length of the tether and  $\vec{J}$  the current through it. As the tether current,  $\vec{J}$ , is in the same direction as the LAO satellite velocity, it follows that

$$qv = LJ \quad (69)$$

Comparing the relevant accelerations gives<sup>17</sup>

$$\frac{q}{m}v = \frac{LI}{m + \lambda L} \quad (70)$$

where  $\lambda$  is the mass per unit length of the tether and  $I$  is the current through the tether. Solving for the length of tether required to approximate an LAO satellite of charge  $q$  and mass  $m$  gives

$$L = \frac{qv}{I - \frac{q}{m}v\lambda} \quad (71)$$

As the tether length cannot be negative, the denominator of this equation must be positive, giving rise to a minimum required tether current of

$$I = \frac{q}{m}v\lambda \quad (72)$$

For a polar GT-1 LAO satellite at an altitude of 400 km with a charge to mass ratio of 2.83 C/kg, and using the aluminum tether presented in Forward, et al.,<sup>17</sup> the absolute minimum current required for a tether to reproduce GT-1 behavior is 43.4 A. However, at this current an infinitely long tether is required. For a more reasonable tether length of 20 km and a spacecraft base mass of 10 kg, a 55 A current is required. A thin aluminum tether will not be able to hold this kind of current.

One slight correction to the above analysis is the self-capacitance of the tether. As a voltage is applied to the long wire, it builds up a charge, causing it to become an LAO satellite itself. Using  $4\pi\epsilon_0 L$  as the capacitance of a wire, a correction to the current limit presented above of the form

$$I = \frac{q}{m}v\lambda - 4\pi\epsilon_0 V_t \quad (73)$$

must be applied, where  $V_t$  is the tether potential. The resistance of the tether is relatively small, creating driving voltages on the order of 1 to 100 kV. These voltages only correct the minimum current by values of 0.1 to 10  $\mu\text{A}$ .

## V. Numerical Simulation

A numerical simulation is developed to test several of the above results. The simulation is a Runge-Kutta (4,5) integration of the sixth-order system defined by Eqs. 7-9, performed by MATLAB®. The simulation is valid for any orbit for a charged satellite in a non-tilted dipole field. The results of two different situations are presented here. First, a polar, circular orbit is calculated, using the charge to mass calculated for GT-1 orbit. Second, an elliptical, equatorial orbit is integrated with constant charge.

Table 1 shows the set of physical parameters common to all simulations.

**Table 1. Physical parameters common to all simulations.**

Parameter	Value
$\omega_E$	7.272e-5 rad/s
$\mu$	3.986e14 m <sup>3</sup> /s <sup>2</sup>
$B_0$	-8.000e15 Wb-m

### A. Polar Circular Orbit

The polar, circular orbit is integrated from the initial conditions in Table 2. The charge-to-mass ratio of 2.831 is chosen based on Eq. 42. Figure 4 shows the resulting orbital path. This path is plotted in a frame that rotates with the Earth so as to highlight the GT-1 nature of the orbit. The orbit is shown to scale with the image of the Earth. Figure 4 shows a slight deviation from a perfect GT-1 orbit. This discrepancy is explained by Fig. 5. This figure compares the forces acting on the satellite. The magnitudes of both gravity and experienced Lorentz force are shown. In this GT-1 polar scenario, we see that the Lorentz force is quite significant with respect to gravity, and this causes some perturbations that erode earlier assumptions. A large Lorentz force causes the orbital eccentricity to be non-zero, creates wobbles in the inclination, and keeps the orbital speed from being constant. These perturbations on the orbit cause slight inaccuracies in the expressions derived above related to a polar circular orbit.

**Table 2. Initial conditions for polar, circular orbit.**

Property	Value
Altitude	400 km
$\frac{q}{m}$	2.831 C/kg
Integration Time	5 orbits

However, the small difference in calculated and desired right ascension angles is due only to wind up of small errors in predicted right ascension rate over time. Figure 6 show both the numerically calculated and

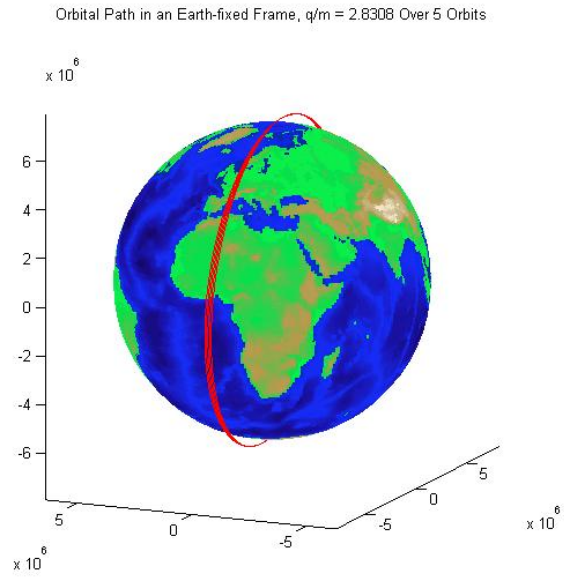


Figure 4. Track of a GT-1 LAO orbit in a frame rotating with Earth.

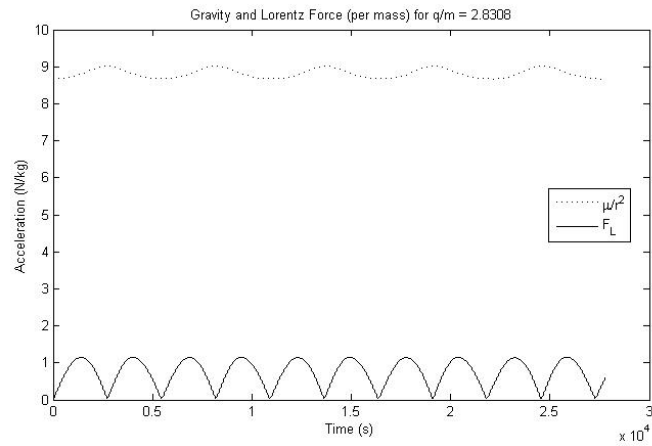


Figure 5. Comparison of gravitational to Lorentz force magnitudes for a GT-1 LAO orbit.

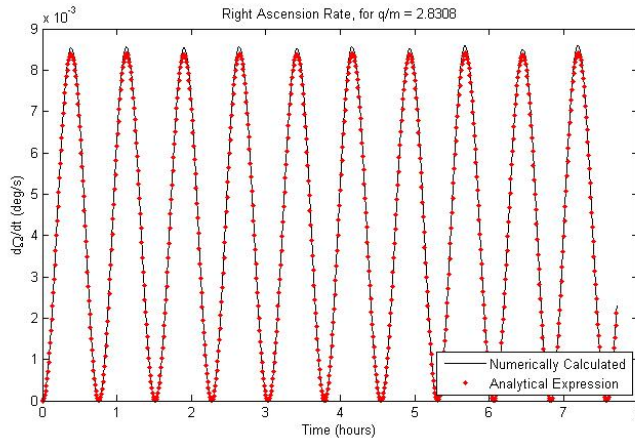


Figure 6. Time rate of change in right ascension for a GT-1 LAO orbit.

the analytically derived right ascension angle rates. The analytical results are based on the expression in Eq. 37; the numerical result is based upon changes in the angular momentum vector of the orbit determined from the state of the system at any given time. These two expressions match nearly exactly, with extremely small, but persistent, errors. As expected, the right ascension rate is zero as the satellite crosses the equator, and large and positive as it crosses the poles. The average values of these expressions is greater than zero, causing a secular increase in the right ascension of the orbit. This increase is shown in Fig. 7, which presents the calculated right ascension angle. These values are produced using the direction of the angular momentum

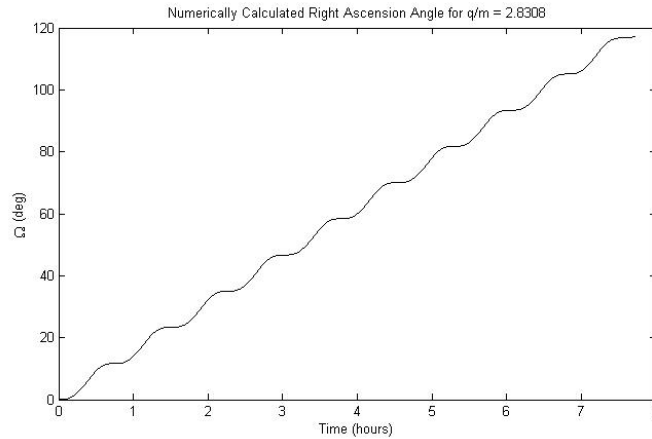


Figure 7. Right ascension angle of a GT-1 LAO orbit.

of the orbit, calculated at each time step. In practice, closed-loop control of the charge might be used to trim these errors that arise due to unmodeled dynamics in the open-loop system.

Finally, Fig. 8 shows the time rate of change of orbital energy throughout the simulation. The solid line represents the numerically calculated energy change based on the state vector at each time, and the dotted line represents the derived expression shown in Eq. 19. These two curves match closely. However, the energy change is centered around zero, and thus there is no secular change in the orbital energy.

## B. Equatorial Orbit, Constant Charge

The equatorial, eccentric, constant charge simulation is initialized using the values shown in Table 3, using the same model as in the case of the polar orbit. The chosen value of  $\frac{q}{m}$  is designed to produce an Earth-



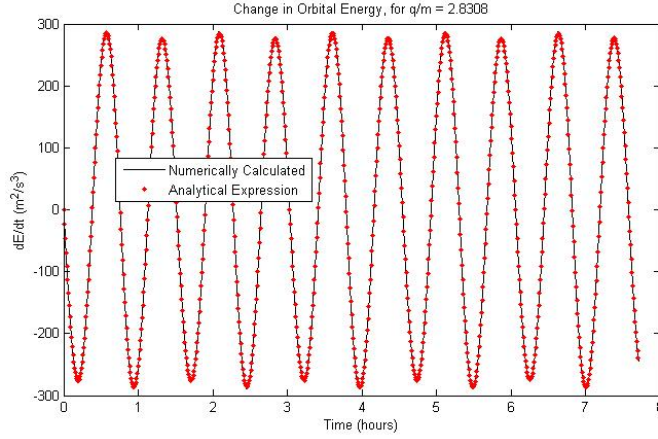


Figure 8. Time rate of change of orbital energy for a GT-1 LAO orbit.

Table 3. Initial conditions for equatorial, constant charge integration.

Property	Value
Perigee Altitude	400 km
Apogee Altitude	1500 km
Eccentricity	0.075
Semimajor Axis	7328 km
$\frac{q}{m}$	-1.774 C/kg
Integration Time	1 day

synchronous motion of the perigee of the orbit. The value is determined using Eq. 60 with a desired rotation rate designed to match the Earth’s rotation, or  $\dot{\omega}_{des} = \omega_E$ .

Figure 9 shows the orbital path of the satellite over one day. Again, the orbit is to scale with the depiction of the Earth as viewed from above the North Pole. The orbital path is shown in a coordinate system rotating with the Earth. The green star on this plot represents the starting point of the integration, which is at the initial perigee.

The rotating frame view in Fig. 9 shows that the charge to mass ratio used in the simulation was not large enough to perfectly cancel the Earth’s rotation with perigee motion. If the correct charge was used the rotating frame view would only show a single curve. Figure 10 shows the numerically calculated and analytically derived arguments of perigee for this case. The numerical values are represented by the solid line. The dotted represents the analytical values, calculated by numerically integrating Eq. 56. While these two curves match quite precisely, we see that the perigee angle does not reach  $360^\circ$  after one day as intended. The results of Fig. 10 give us confidence in the result for time rate of change of perigee expressed in Eq. 56, but show that accuracy is lost in integrating this result to obtain Eq. 60. In that integration, we assumed that the semimajor axis and eccentricity were changing slowly enough that we could assume the both  $a$  and  $e$  were not explicit functions of true anomaly  $\nu$ . However, the charge-to-mass ratios are large enough in this case to make that a poor assumption. However, for smaller desired perigee rate, like mitigating J2 effects, Eq. 60 is quite accurate. Creating the Earth-synchronous effect is certainly possible; it just requires a larger  $\frac{q}{m}$  than predicted. Creating a closed-loop control system to adjust  $\frac{q}{m}$  can account for this variation, in addition to correcting for imperfections in the magnetic field model, plasma variations, etc. Equation 60 represents a starting point for design and a base to wrap a controller around.

The curves depicted in Fig. 11 represent the time rate of change of orbital energy for the LAO satellite. Again the numerical values are represented by a solid line, and are calculated based on the work done on the satellite by the Lorentz force at any given time. The dotted curve shows the analytical result based on the

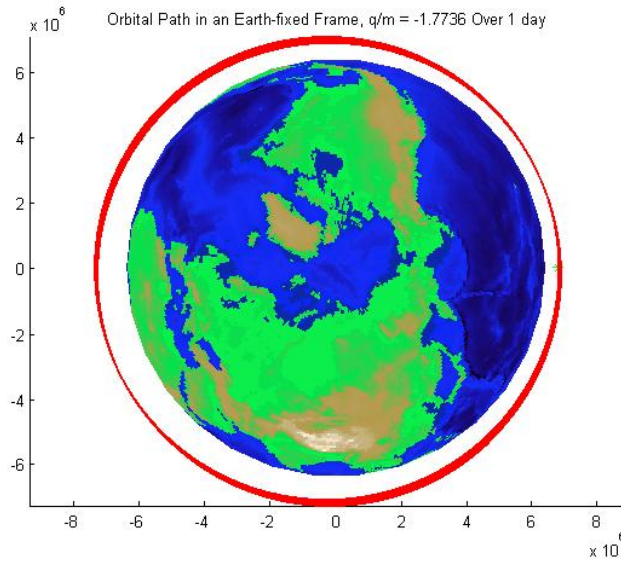


Figure 9. Earth-fixed orbital path of an equatorial, constant charge LAO satellite with  $\frac{q}{m}$  calculated for synchronous perigee movement.

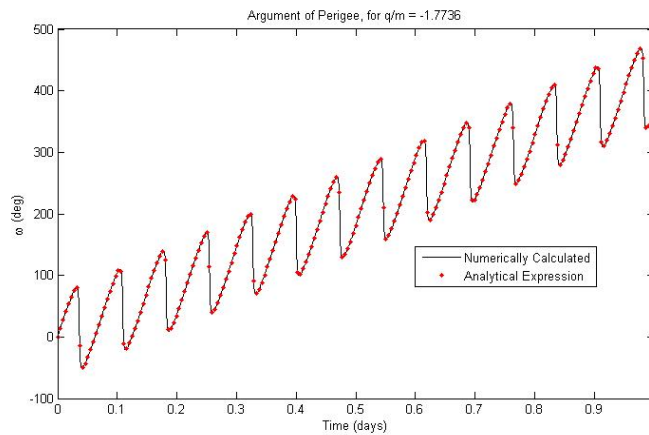


Figure 10. Perigee angle of an equatorial, constant charge LAO satellite.

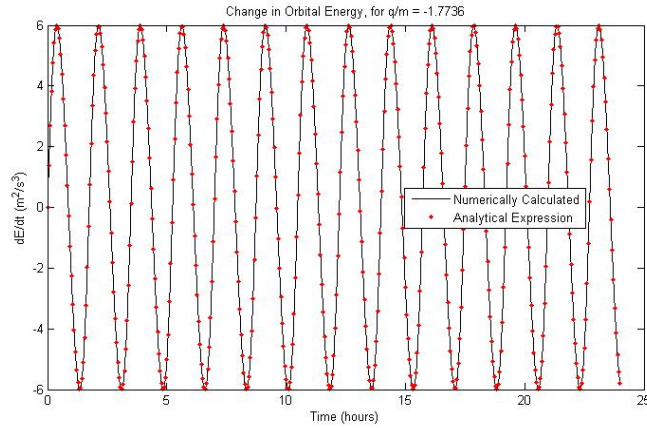


Figure 11. Time rate of change of orbital energy for an equatorial, constant charge LAO satellite.

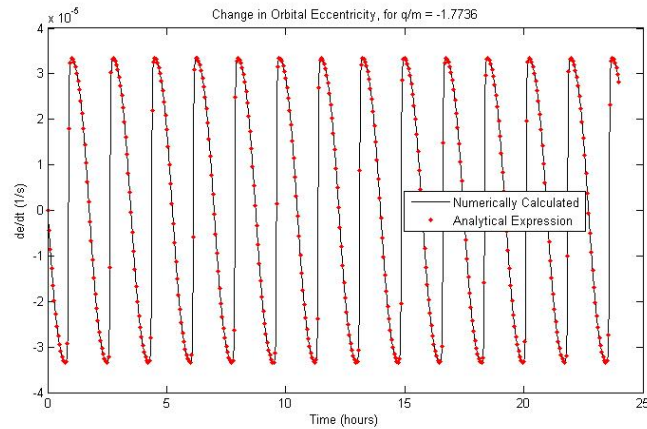


Figure 12. Time rate of change of orbital eccentricity for an equatorial, constant charge LAO satellite.

expression in Eq. 47. These two curves agree nearly exactly, showing an energy change that is zero-mean. As expected, the largest changes in  $E$  occur around perigee, with smaller effects near apogee.

Figure 12 shows changes in orbital eccentricity over the length of the simulation. The solid curve is a numerical differentiation of the eccentricity calculated at each time step. The dotted line is the result of applying Eq. 54. The results are well matched, nominally zero-mean, and exhibit much larger changes around perigee than apogee.

Thus, we see that a constant charge, equatorial LAO satellite can have an arbitrary time rate of change of argument of perigee. The required charge-to-mass ratio for a desired rate depends solely on the initial orbit configuration and the magnitude of the desired change. The orbital energy and eccentricity also change in a predictable manner, but with no secular variations.

These simulations have shown excellent agreement between the derived equations of motion and the analytical expressions for the orbital changes created by the LAO system. We see that useful and desirable changes can be made to orbits using this system. Although only simulations of polar and equatorial orbits are presented here, an arbitrarily inclined orbit will just combine the properties of these two results in some way. Additionally, only constant charges are examined here. Simple charge controls can be applied to produce secular changes in any of the perturbations equations presented above. For closer examination of the nonconstant charge case see Atchison.<sup>18</sup>

## VI. Effects of a Tilted Dipole Magnetic Field

The above analysis assumes the geomagnetic field to be a dipole field whose magnetic north pole is aligned with the Earth's geographic north pole. While this assumption allows for several clean analytical results to be calculated, a more accurate model of the geomagnetic field is a dipole field whose north pole axis is tilted with respect to true north. The actual geomagnetic north pole sits in northern Canada, tilted roughly  $10^\circ$  from geographic north.

To implement a tilted dipole model, two new parameters are defined:  $\alpha$  represents the angle between the magnetic north pole and geographic north pole, and  $\Omega_m$  represents the longitude of the magnetic north as measured from the inertial  $x$ -axis. As the geomagnetic field is locked into the Earth's rotation,  $\Omega_m$  varies with respect to time as  $\omega_E t + \Omega_m(0)$ . The same general perturbation procedures as above is applicable to the tilted dipole case. Applying the vector model of a dipole field,  $\vec{B} = \frac{B_0}{r^3} [3(\hat{N} \cdot \hat{r})\hat{r} - \hat{N}]$  where  $\hat{N}$  is a unit vector along the magnetic north pole, to the general energy change equation, Eq. 14, yields a new energy-change relationship based on a tilted dipole:

$$\begin{aligned} \dot{E} = \frac{q}{m} \omega_E B_0 \sqrt{\mu} \frac{[1 + e \cos(u - \omega)]^2}{[a(1 - e^2)]^{5/2}} & \left\langle 2 \sin i (\cos u + e \cos \omega) \right. \\ & \times \{ \cos(\Omega_m - \Omega) \sin \alpha \cos u + \sin(\Omega_m - \Omega) \cos i \sin \alpha \sin u + \sin i \cos \alpha \sin u \} \\ & - e \sin(u - \omega) [3 \sin u \sin i \{ \cos(\Omega_m - \Omega) \sin \alpha \cos u \\ & + \sin(\Omega_m - \Omega) \cos i \sin \alpha \sin u + \sin i \cos \alpha \sin u \} - \cos \alpha] \left. \right\rangle \end{aligned} \quad (74)$$

This expression is for a general elliptical orbit in a dipole field with any tilt. Equation 74 includes the non-tilted dipole case and encompasses the expressions in Eqs. 19 and 47. A similarly long expression can be derived for angular momentum change, which is not presented here for the sake of brevity.

The effects of adding a tilt-angle to the dipole field are numerically simulated based on a generalization of the above integrations. The results of two simulations comparing the non-tilted dipole and the tilted dipole are shown in Fig. 13. This figure shows two integrations, both beginning with same initial conditions,

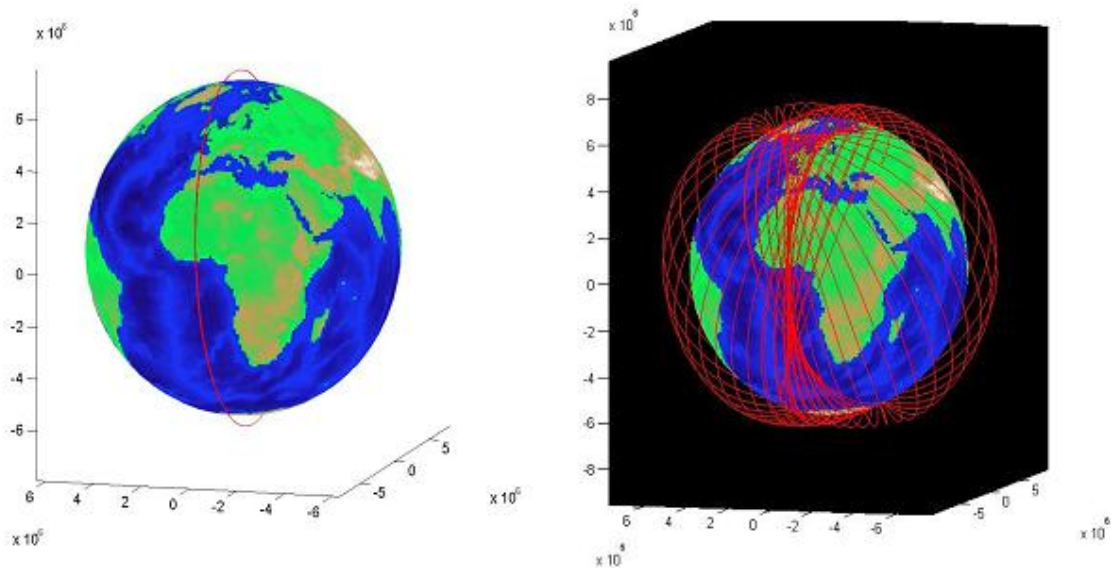


**Figure 13. Comparison between two integration with the same initial conditions. The left plot uses a non-tilted dipole field; the right used a dipole field tilted to  $10^\circ$ .**

namely a 400 km altitude polar circle with a charge-to-mass ratio calculated to give GT-1 behavior. The results are plotted in an Earth-fixed coordinate system. The left plot shows the integration in a non-tilted dipole, giving the familiar GT-1 orbit. The right plot displays the result of a simulation including a dipole

field tilted at angle of  $10^\circ$ . This orbit is quickly driven away from GT-1 behavior to no readily identifiable orbit.

The cause of this deviation is found in the terms in Eq. 74 arising from the tilted dipole. In particular, the term of the form

$$\dot{E} \propto \cos(\Omega_m - \Omega) \sin \alpha \sin i \cos^2 u \quad (75)$$

causes a secular drift in the energy of the orbit away from its initial value. Initially the quantity  $\cos(\Omega_m - \Omega)$  is constant, as this condition embodies the LAO GT-1 behavior. A term similar to Eq. 75 also arises in the change in angular momentum expression. Thus, as the orbit continues,  $E$  and  $\vec{h}$  drift away from their nominal values, causing the spacecraft charge-to-mass ratio to be unsuitable for GT-1 behavior. As the orbit moves away from the GT-1 behavior,  $\Omega_m - \Omega$  is no longer constant, and the spacecraft settles into a periodic motion that does not resemble GT-1.

The expression in Eq. 75 should go to zero when  $\Omega_m - \Omega = \pm 90^\circ$ . Figure 14 shows a numerical simulation of both of these initial orbit longitudes. Each of the two plots in this figure shows the orbital energy of

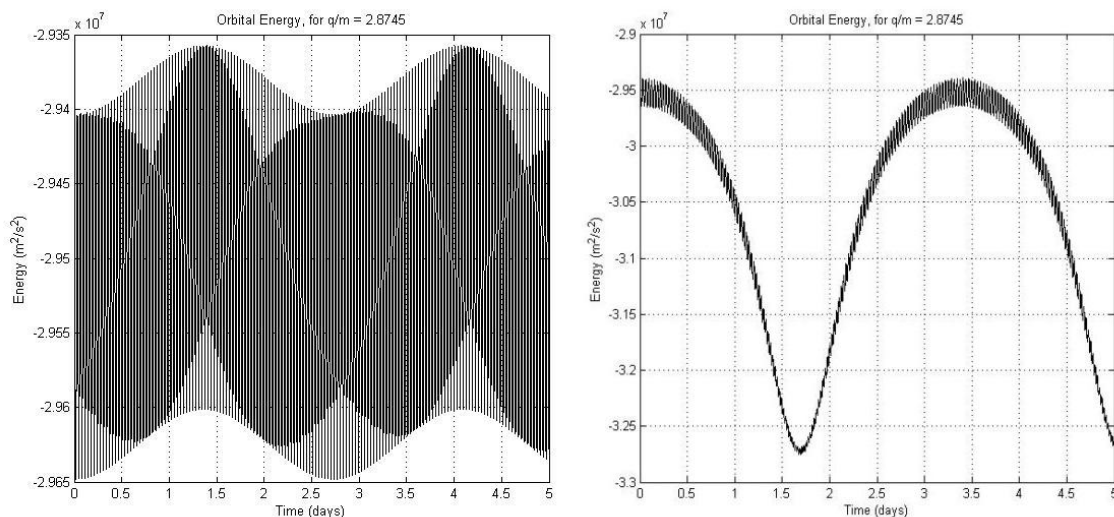


**Figure 14.** The orbital energy of two tilted dipole integrations with a  $\frac{q}{m}$  set to give GT-1 behavior. The left plot is for  $\Omega_m - \Omega = -90^\circ$ . The right shows an initial angle of  $\Omega_m - \Omega = +90^\circ$ .

the spacecraft throughout the simulation. The left plot shows  $\Omega_m - \Omega = -90^\circ$ , while the right displays  $\Omega_m - \Omega = +90^\circ$ . In the  $-90^\circ$  case, the orbital energy remains nearly constant, and the spacecraft remains close to the intended GT-1 region. However, in the  $+90^\circ$  case, the energy varies over a large amount, and the satellite does not maintain GT-1. This behavior can be attributed to the sign changes that  $\cos(\Omega_m - \Omega)$  makes around  $\pm 90^\circ$ . At  $-90^\circ$ , the sign of the cosine function switches in such a way to push the orbital energy back towards its nominal value. At  $+90^\circ$ , the opposite happens. Essentially,  $\Omega_m - \Omega = -90^\circ$  is a stable equilibrium and  $\Omega_m - \Omega = +90^\circ$  is an unstable equilibrium.

Solutions near  $\Omega_m - \Omega = -90^\circ$  remain bounded, but periodic, in the quantity  $\Omega_m - \Omega$ . The error in  $\Omega_m - \Omega$  increases as the initial value of  $\Omega_m - \Omega$  gets further from  $-90^\circ$ , until the system becomes unstable at  $\Omega_m - \Omega = 0^\circ$  or  $180^\circ$ . For the LAO GT-1 concept to be a viable application, a nearly constant arbitrary value of  $\Omega_m - \Omega$  should be maintainable. However, due to symmetry of the polar orbit, a range of only  $180^\circ$  of  $\Omega_m - \Omega$  allows for full longitudinal coverage. Thus, only the bounded-error cases of  $180^\circ < \Omega_m - \Omega \leq 360^\circ$  must be considered. Allowing for the modulation of charge in some controlled sense should enable the reduction of error in these cases to a reasonable amount.

## VII. Conclusion

Lorentz Augmented Orbits are based on simple physical principles but can be used to accomplish a variety complex orbital behaviors. Analytical results, verified by numerical simulations, show the effects of

the Lorentz force on the orbit of an LAO satellite. The resulting changes in orbital elements can be used to develop novel applications for the LAO system. These new applications include polar, single-orbit repeat-groundtrack (GT-1) satellites. These orbits can exist at any altitude, not just the traditional GEO height. We show from first principles a simple expression for the charge-to-mass ratio required for such a feat. This expression is verified numerically and allows for missions designs to be evaluated. A successfully implemented GT-1 LAO orbit would greatly outperform today's imaging satellites. Also numerically confirmed is the existence of equatorial orbits with arbitrary control over the location of perigee. Again, a simple expression for the charge required is shown from first principles. These orbits can create an Earth-synchronous orbit whose perigee and apogee lie at a constant longitude. The above applications rely on merely maintaining a constant charge to mass on the satellite; many further applications can be developed for fully controlling the charge based on the various expressions for orbital element change presented here.

Many avenues for future work exist within the LAO framework. The dynamics of the system based on a tilted dipole field will be examined in more depth. The results given here can easily be applied to spacecraft formation flying systems. The addition of controlled charge modulation promises to broaden the applicability of LAO.

## Acknowledgments

This work was supported by the NASA Institute for Advanced Concepts and the National Science Foundation IGERT Program in Nonlinear Systems at Cornell.

## References

- <sup>1</sup>Wertz, J. R. and Larson, W. J., *Space Mission Analysis and Design*, Microcosm Press, El Segundo, 1999.
- <sup>2</sup>Peck, M. A., "Prospects and Challenges of Lorentz-Augmented Orbits," *Proceedings of the AIAA Guidance, Navigation, and Control Conference*, August 2005.
- <sup>3</sup>Cosmo, M. L. and Lorenzini, E. C., *Tethers in Space Handbook Third Edition*, NASA Marshall Spaceflight Center, Huntsville, AL, 1997.
- <sup>4</sup>Rothwell, P. L., "The superposition of rotating and stationary magnetic sources: Implications for the auroral region," *Physics of Plasmas*, Vol. 10, No. 7, 2003, pp. 2971–2977.
- <sup>5</sup>Schaffer, L. and Burns, J. A., "The Dynamics of Weakly Charged Dust: Motion Through Jupiter's Gravitational and Magnetic Fields," *Journal of Geophysical Research*, Vol. 92, 1987, pp. 2264–2280.
- <sup>6</sup>Schaffer, L. and Burns, J. A., "Charged Dust in Planetary Magnetospheres: Hamiltonian Dynamics and Numerical Simulations for Highly Charged Grains," *Journal of Geophysical Research*, Vol. 99, 1994, pp. 17211–17223.
- <sup>7</sup>Mullen, E. G., Gussenhoven, M. S., and Hardy, D. A., "SCATHA Survey of High-Voltage Spacecraft Charging in Sunlight," *Journal of the Geophysical Science*, Vol. 91, 1986, pp. 1074–1090.
- <sup>8</sup>Garrett, H. B. and Whittlesey, A. C., "Spacecraft Charging, An Update," *IEEE Transactions on Plasma Science*, Vol. 28, No. 6, 2000, pp. 2017–2028.
- <sup>9</sup>Schaub, H., Parker, G. G., and King, L. B., "Challenges and Prospects of Coulomb Spacecraft Formations," *Proceedings of the AAS John L. Junkins Symposium*, May 2003.
- <sup>10</sup>Lai, S. T., "An Overview of Electron and Ion Beam Effects in Charging and Discharging of Spacecraft," *IEEE Transactions on Nuclear Science*, Vol. 36, No. 6, 1989, pp. 2027–2032.
- <sup>11</sup>Hough, M. E., "Lorentz Force Perturbations of A Charged Ballistic Missile," *Proceedings of the AIAA Guidance and Control Conference*, August 1982.
- <sup>12</sup>Schaub, H., "Stabilization of Satellite Motion Relative to a Coulomb Spacecraft Formation," *Journal of Guidance, Control, and Dynamics*, Vol. 28, No. 6, 2005, pp. 1231–1239.
- <sup>13</sup>Kong, E., Kwon, D. W., Schweighart, S. A., Elias, L. M., Sedwick, R. J., and Miller, D. W., "Electromagnetic Formation Flight for Multisatellite Arrays," *Journal of Spacecraft and Rockets*, Vol. 41, No. 4, 2004, pp. 659–665.
- <sup>14</sup>Tikhonov, A. A., "A Method of Sempassive Attitude Stabilization of a Spacecraft in the Geomagnetic Field," *Cosmic Research*, Vol. 41, No. 1, 2003, pp. 69–79.
- <sup>15</sup>Van de Graaf, R. J., Compton, K. T., and Van Atta, L. C., "The electrostatic production of high voltage for nuclear investigations," *Physical Review*, Vol. 43, No. 3, 1933, pp. 149–157.
- <sup>16</sup>Burns, J. A., "Elementary derivation of the perturbation equations of celestial mechanics," *American Journal of Physics*, Vol. 44, No. 10, 1976, pp. 944–949.
- <sup>17</sup>Forward, R. L., Hoyt, R. P., and Uphoff, C., "The Terminator Tether: A Low-Mass System for End-of-Life Deorbit of LEO Spacecraft," *Tether Technical Interchange Meeting*, 1997.
- <sup>18</sup>Atchison, J., Streetman, B., and Peck, M. A., "Lorentz Augmented Capture at Jupiter," *Proceedings of the AIAA Guidance, Navigation, and Control Conference (Submitted)*, August 2006.